JACS
JOURNAL OF THE AMERICAN CHEMICAL SOCIETY
pubs.acs.org/JACS
Article

β-Bracelets: Macrocyclic Cross-β Epitope Mimics Based on a Tau Conformational Strain

Benjamin H. Rajewski, Kamlesh M. Makwana, Isaac J. Angera, Danielle K. Geremia, Anna R. Zepeda, Grace I. Hallinan, Ruben Vidal, Bernardino Ghetti, Arnaldo L. Serrano, and Juan R. Del Valle*

Cite This: J. Am. Chem. Soc. 2023, 145, 23131−23142
Read Online
ACCESS | Metrics & More | Article Recommendations | Supporting Information

ABSTRACT: The aggregation of misfolded tau into neurotoxic fibrils is linked to the progression of Alzheimer's disease (AD) and related tauopathies. Disease-associated conformations of filamentous tau are characterized by hydrophobic interactions between side chains on unique and distant β-strand modules within each protomer. Here, we report the design and diversity-oriented synthesis of β-arch peptide macrocycles composed of the aggregation-prone PHF6 hexapeptide of tau and the cross-β module specific to the AD tau fold. Termed "β-bracelets", these proteomimetics assemble in a sequence- and macrocycle-dependent fashion, resulting in amyloid-like fibrils that feature in-register parallel β-sheet structure. Backbone N-amination of a selected β-bracelet affords soluble inhibitors of tau aggregation. We further demonstrate that the N-aminated macrocycles block the prion-like cellular seeding activity of recombinant tau as well as mature fibrils from AD patient extracts. These studies establish β-bracelets as a new class of cross-β epitope mimics and demonstrate their utility in the rational design of molecules targeting amyloid propagation and seeding.

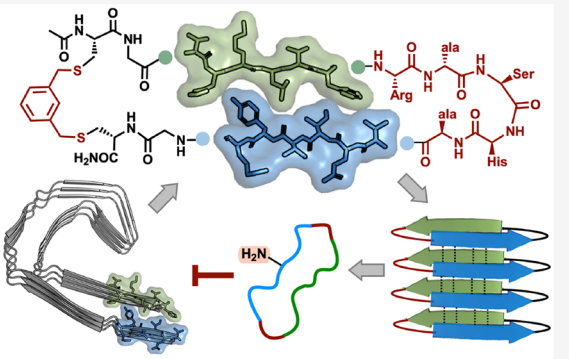

INTRODUCTION

Fibrillar amyloid deposits composed of β-sheet-rich protein assemblies are a hallmark of several neurodegenerative diseases.[1,2] A common feature of these fibrils is the presence of cross-β interactions, wherein a steric zipper is formed by interdigitation of side chains from opposing β-strands that are aligned perpendicular to the fibril axis.[3] Intermonomer H-bonding along the strand edges leads to the growth of toxic fibrils composed of misfolded proteins. Tau is an intrinsically disordered microtubule-associated protein that can transition to cross-β amyloid structure following aberrant post-translational modification or mutations in the *MAPT* gene.[4−8] Tau plays a role in maintaining neuronal microtubule dynamics, cellular signaling, and mRNA translation; however, its misfolding is strongly linked to Alzheimer's disease (AD), corticobasal degeneration (CBD), progressive supranuclear palsy (PSP), and several other tauopathies. Additionally, tau oligomers and fibrils secreted from diseased neurons are capable of seeding the aggregation of tau within healthy cells in a prion-like manner.[9−12] Molecules designed to probe tau propagation and seeding could shed light on the mechanisms of tauopathic progression and aid in the development of diagnostic or disease-modifying ligands.

There are currently no tau-targeted therapies approved for clinical use, though many groups have worked to develop direct inhibitors of tau aggregation based on small molecules, dyes, and peptides.[13−16] Targeting tau interactions with peptide derivatives offers certain advantages, due in part to their ability to contact a large surface interface and mimic the β-strand secondary structure characteristic of amyloids.[17] Computationally aided *de novo* design and phage display library screening have afforded several peptide-based tau inhibitors.[18−27] Considerable effort has also been devoted to mimicry of the aggregation-driving $_{275}$VQIINK$_{280}$ (PHF6*) and $_{306}$VQIVYK$_{311}$ (PHF6) hexapeptides located in the second and third microtubule-binding repeat domains of tau.[28−30] Incorporation of PHF6 motifs into macrocyclic β-hairpin[31,32] and cyclotide scaffolds[33] resulted in compounds that inhibit the aggregation of the hexapeptide PHF6 tau model. More recently, structure-guided residue substitution of PHF6 and PHF6* motifs afforded peptides that inhibit the aggregation of full-length tau and block the cellular seeding activity of patient-derived tau extracts.[34−36] Of note, all the aforementioned tau mimetic approaches present a single recognition strand, and several rely on auxiliary strands or templates to present this module in the appropriate extended conformation.

Received: June 28, 2023
Published: October 16, 2023

https://doi.org/10.1021/jacs.3c06830
J. Am. Chem. Soc. 2023, 145, 23131−23142

Within the past decade, advances in cryo-EM and software-aided fibril reconstruction have afforded unprecedented insight into the structure of pathogenic amyloids.[2,37] These studies are revealing remarkable polymorphism in patient-derived tau extracts and suggest that the conformation of filamentous tau varies by disease.[38−41] An important consequence of this structural diversity is that the PHF6* and PHF6 strands can engage in cross-β interactions with distinct hexapeptide modules, depending on the tauopathy. In some amyloidogenic proteins, the accepted aggregation-prone modules are separated from their interacting cross-β sequences by short, naturally occurring loops composed of 3−7 residues. This feature has allowed for the design of peptide-based mimics of human islet amyloid polypeptide (hIAPP) and β-amyloid (Aβ).[42,43] However, in several tau strains the key aggregation-driving PHF6 motif interacts with cross-β modules that are distant in primary sequence (Figure 1).[38,44,45,40]

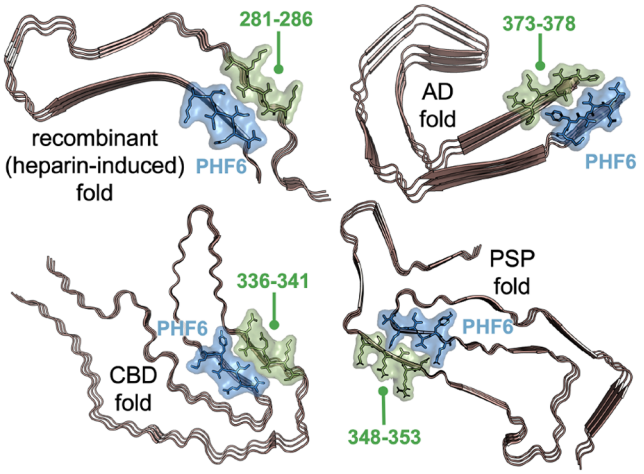

Figure 1. Cryo-EM structures of filaments derived from heparin-induced recombinant tau ("snake" fold; PDB 6QJH) as well as tau extracts from Alzheimer's disease (AD paired filament; PDB 5O3L), corticobasal degeneration (CBD type I; PDB 6TJO), and progressive supranuclear palsy (PSP; PDB 7P65) patient-derived brain tissue. The aggregation-driving PHF6 hexapeptide (blue) and cross-β interacting module (green) are highlighted.

We hypothesized that complete cross-β epitopes, harboring two H-bonding edges and opposing β-strand modules, may serve as conformational mimics of disease-associated tau misfolds. In addition, we envisioned that such mimics could guide the structure-based design of more efficacious tau aggregation inhibitors. Here, we describe a diversity-oriented approach toward peptide macrocycles, termed "β-bracelets", that feature both the aggregation-prone PHF6 sequence and the cross-β interacting modules observed in solid-state structures of tau. Using a combination of biophysical techniques, we demonstrate that an AD tau-based β-bracelet forms higher-order assemblies reminiscent of those in the pathological fold. Moreover, we show that these macrocycles can serve as useful templates for the design of soluble inhibitors of tau aggregation. Backbone-substituted derivatives of an AD tau β-bracelet were found to block aggregation as well as cellular seeding induced by both full-length recombinant proteins and fibrils extracted from AD patient tissue. The described approach represents a new modality to mimic amyloidogenic cross-β epitopes and lays the groundwork for targeting other protein interactions that span a β-solenoid edge.

RESULTS

Design and Synthesis of β-Bracelets Derived from the AD Tau Fold. The assembly of repeating amyloidogenic proteins is driven largely by in-register, intermolecular H-bonds between parallel β-strand edges.[3] The resulting β-arch conformation is further stabilized by hydrophobic interactions at the interface of cross-β motifs within the same protomer. This is distinct from β-hairpin conformations, wherein *intra*molecular edge-to-edge H-bonding occurs between antiparallel strands that are connected through β-turns. The strands in β-arches are instead linked through β-arcs spanning 2−7 residues.[46,47] Although turn and arc conformations often interconvert, Kajava and co-workers observed that arcs composed of 2 or 3 residues do not readily accommodate the 180° reversal required for tight cross-β packing of nearby strands (Figure 2A).[46] The wider strand angle associated with

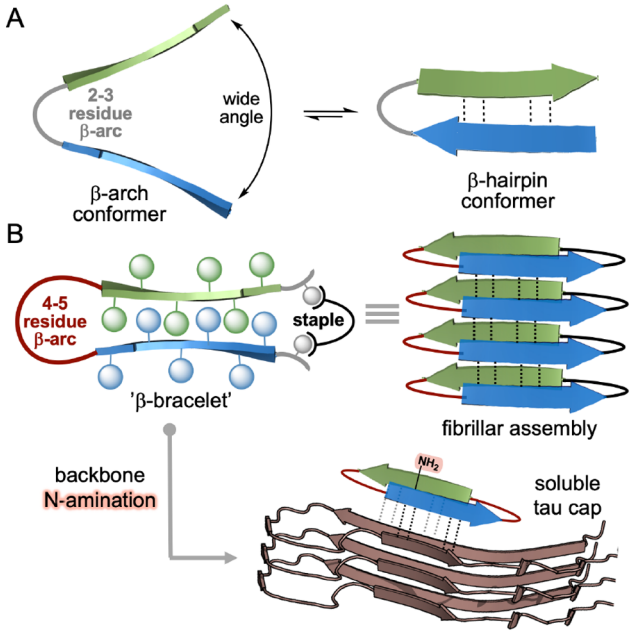

Figure 2. (A) Illustration of the equilibrium between antiparallel β-arch and β-hairpin conformations for a strand−loop−strand peptide. (B) Design of "β-bracelets" stabilized by hydrophobic side-chain packing, larger β-arc motif, and terminal staple. Also depicted are the proposed self-assembly of β-bracelets and conversion into soluble tau inhibitors through backbone amide substitution.

these shorter connectors is frequently observed in β-helix folds as well as in the more common antiparallel β-hairpin conformation. To allow for the cross-β packing observed in fibrillar tau strains, we sought to incorporate a longer β-arc into our proteomimetic design (Figure 2B). To further stabilize the β-arch conformation, we also introduced terminal staples featuring diverse linkers. Effective mimicry of tau epitopes was expected to afford macrocycles that undergo amyloid-like assembly. Conversely, backbone amide substitution would render tau mimics incapable of fibrilization, potentially affording inhibitors of tau propagation.

Tau mimetic peptides based on the high-resolution structure of the AD fibril fold were synthesized on Rink amide MBHA

https://doi.org/10.1021/jacs.3c06830
J. Am. Chem. Soc. 2023, 145, 23131−23142

resin using standard Fmoc solid-phase peptide synthesis protocols (Scheme 1). These macrocycles feature the PHF6

Scheme 1. Solid-Phase Synthesis and Macrocyclization of β-Bracelet Tau Mimics

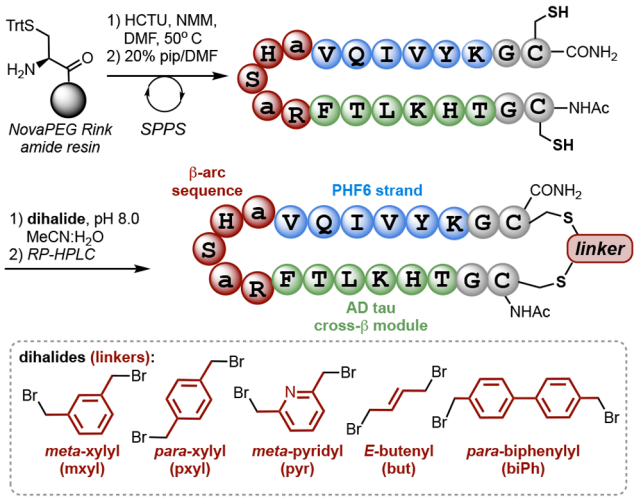

hexapeptide module in addition to the $_{373}$THKLTF$_{378}$ cross-β motif in the AD tau cryo-EM structure.[38] The β-strands were connected using a 5-residue β-arc recently described by Gellman and Woolfson.[48] This "RaSHa" sequence (where a = D-Ala) is based on bioinformatic analysis of motifs that bridge antiparallel strands in known β-solenoid structures and has been shown to accommodate the conformational and distance requirements of an interlayer linker in a mini-amyloid model system. We also appended Gly-Cys dipeptides to the termini to enable bisalkylation with dihalide electrophiles. This diversity-oriented approach would allow us to evaluate several linkers for their ability to accommodate the desired cross-β structure starting from a single linear substrate.

Characterization of β-Bracelet Tau Mimics by ThT Assay and TEM. The ability of macrocyclic tau mimics to undergo amyloid-like self-assembly was first investigated by a thioflavin T (ThT) fluorescence assay. ThT is an amyloid-specific fluorescent dye that binds to channels along the long axis of fibrils composed of β-sheets. We first dissolved each peptide to a final concentration of 25 μM in aq PBS and incubated the samples for 2 d at 37 °C in the presence of 10 μM ThT. Endpoint fluorescence readings from a linear control sequence (**linear-AD**) and 5 macrocyclic analogues showed that the incorporation of terminal tethers results in enhanced ThT signal (Figure 3A). Moreover, ThT in the presence of the *p*-biphenyl- and *m*-xylyl-linked macrocycles (**biPh-AD** and **mxyl-AD**) gave rise to considerably higher fluorescence relative to the linear sequence. Interestingly, the *p*-xylyl-linked AD macrocycle (**pxyl-AD**) resulted in fluorescence ~5-fold lower than that of its isomeric **mxyl-AD** analogue, suggesting that subtle changes in the linker geometry can significantly impact fibrilization and ThT binding. We also synthesized a scrambled analogue of the *m*-xylyl macrocycle (**scrm-AD**), in which the terminal Cys residues, aryl linker, and β-arc were maintained but residues within the β-strand modules were swapped across the register (Figure S1). In the presence of ThT, this analogue resulted in the lowest fluorescence within the series.

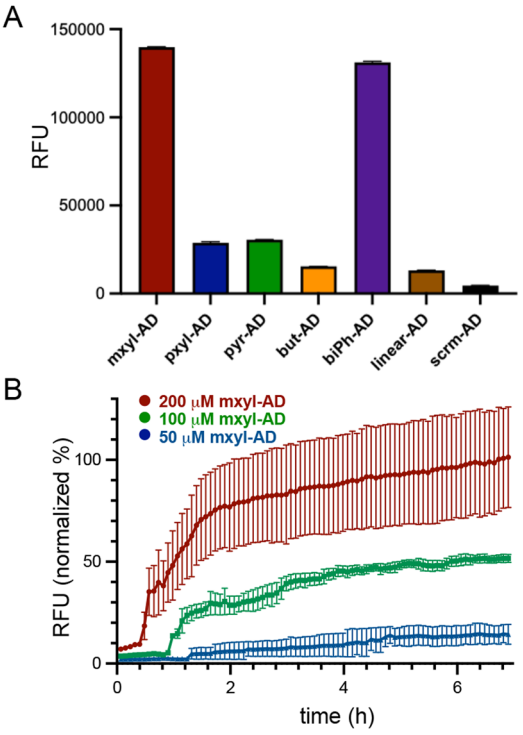

Figure 3. (A) Endpoint ThT fluorescence of AD tau mimics at 25 μM in aq PBS after 48 h. (B) Time and concentration dependence of **mxyl-AD** fibrilzation in aq PBS, monitored by ThT fluorescence (fluorescence intensity is normalized to the maximum fluorescence observed for 200 μM **mxyl-AD**).

While most of the macrocycles exhibited higher ThT fluorescence relative to **linear-AD** immediately upon dissolution in PBS buffer, we found that heating a stock solution of **mxyl-AD** in water to 90 °C was effective in reducing the initial ThT-positive fluorescence. Time-course experiments with **mxyl-AD** diluted with aq PBS revealed a short lag phase as well as a concentration-dependent increase in maximum fluorescence over 7 h (Figure 3B). The presence of a buffer was critical for aggregation. A sample of **mxyl-AD** incubated in unbuffered water did not exhibit fluorescence but could be induced to aggregate upon addition of aq PBS during the course of the assay (Figure S2).

Transmission electron microscopy (TEM) was then used to verify the growth of fibrils after 4 days of incubation of **mxyl-AD** at 50 μM in aq PBS. Consistent with the ThT assay, we observed the formation of filaments within networks of fibrils (Figure 4). In contrast, incubation of **linear-AD** and **scrm-AD** resulted in only sparsely distributed amorphous aggregates, as determined by TEM. Taken together, these data suggest that fibrilization of our tau mimics is sequence-, macrocycle-, and linker-dependent. Interestingly, macrocyclization with the *m*-xylyl linker also enhanced the self-assembly of mimics in which the AD-derived $_{373}$THKLTF$_{378}$ motif was replaced with cross-β sequences from recombinant and corticobasal degeneration tau folds (Figure S3). In these cases, we also observed high ThT fluorescence relative to linear controls and dense networks of mature fibrils by TEM (Figures S4 and S5).

Characterization of mxyl-AD by Circular Dichroism. Although the N-terminally acetylated PHF6 hexapeptide is known to assemble into cross-β fibrils *in vitro*, we sought to characterize the conformational transition of the **mxyl-AD**

https://doi.org/10.1021/jacs.3c06830
J. Am. Chem. Soc. 2023, 145, 23131−23142

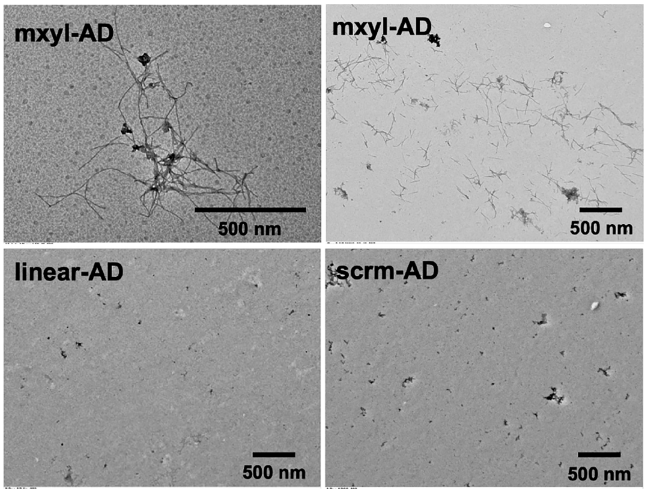

Figure 4. Representative TEM images of **mxyl-AD**, **linear-AD**, and **scrm-AD** after 4 days of incubation at 50 μM in aq PBS (scale bars = 500 nm).

macrocycle upon aggregation by far-UV circular dichroism (CD) spectroscopy. Incubation of **mxyl-AD** in aq PBS resulted in the formation of insoluble aggregates that made it difficult to obtain a clear CD spectrum following self-assembly. However, a sample of **mxyl-AD** dissolved directly in unbuffered water exhibited a random coil structure, as determined by CD (Figure 5). We then collected the insoluble fraction of **mxyl-AD** following fibrilization in aq PBS and redissolved the pellet in water. The CD spectrum of this solution exhibited a clear β-sheet signature with a pronounced minimum at 221 nm. This indicates that, similar to PHF6 and full-length tau, **mxyl-AD** transitions to a β-sheet-rich conformation upon fibrilization in buffered aqueous solution.

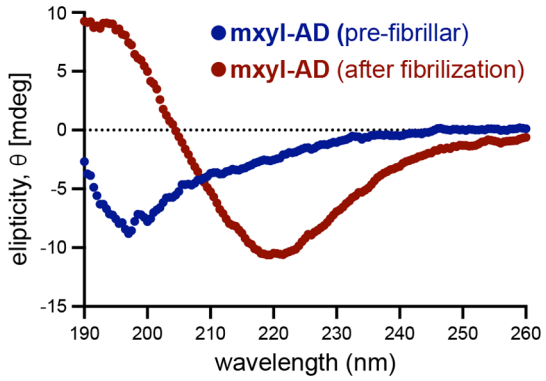

Figure 5. CD spectra of **mxyl-AD** dissolved directly in H_2O (blue) or following fibrilization in aq PBS, pelleting, and resuspension in H_2O (red).

The **mxyl-AD** macrocycle incorporates a β-arc solenoid linker in addition to the natural cross-β module from AD tau. Our design was thus expected to favor a mini-amyloid structure featuring *inter*molecular parallel β-sheet interactions, in contrast to the *intra*molecular edge−edge interactions between antiparallel strands connected through β-turns. Although accurate estimation of parallel versus antiparallel β-sheet structure has been difficult to achieve with CD, Kardos and co-workers recently reported a secondary structure prediction algorithm (BeStSel) to distinguish between topologically distinct β-rich proteins and amyloid fibrils.[49] Using BeStSel in conjunction with post-fibrillar **mxyl-AD** CD data yielded an estimated parallel β-sheet content of 70%. This secondary structure component far outweighed predicted contributions from α-helical (23%) and antiparallel β-sheet (7%) structures. Qualitatively, the red-shifted minimum band (221 nm) in the CD spectrum of **mxyl-AD** after fibrilization is also consistent with other theoretically calculated and experimentally determined parallel β-sheet structures.[49−51]

Characterization of mxyl-AD by Two-Dimensional Infrared Spectroscopy. To further support our proposed model of supramolecular association for **mxyl-AD**, we employed two-dimensional infrared (2D IR) spectroscopy. When combined with isotope labeling, 2D IR spectroscopy provides a means to differentiate between parallel and antiparallel β-sheet interactions involving the backbone carbonyl groups (Figure 6A).[52] A $^{13}C/^{18}O$ vibrational probe placed on a single peptide residue yields a considerable frequency shift, isolating it from the rest of the amide-I vibrational region. These individual isotope labels, when aligned in a parallel β-sheet, can couple together to form a linear chain of oscillators, red-shifting the label frequency down from the uncoupled values of 1585−1595 cm^{-1}.[53]

We selected the central V17 residue in **mxyl-AD** (corresponding to V309 in tau) for isotope labeling and synthesized the $^{13}C/^{18}O$-**mxyl-AD** derivative for comparison by 2D IR spectroscopy. As shown in Figure 6B, the unlabeled **mxyl-AD** spectrum exhibits an amide-I peak at 1619 cm^{-1} (pump frequency), signifying predominantly amyloid β-sheet structure.[54] Figure 6C shows the Val-labeled $^{13}C/^{18}O$-**mxyl-AD** spectrum with new peaks appearing at 1573 and 1595 cm^{-1}. The 1595 cm^{-1} peak is consistent with uncoupled labels, while the 22 cm^{-1} shift down to 1575 cm^{-1} suggests a coupling constant of about 11 cm^{-1}. This value is consistent with the interstrand coupling of an in-register parallel β-sheet.[53,55] The presence of an uncoupled 1595 cm^{-1} peak suggests that some population of the macrocycle either is unaggregated or adopts an alternative structure in the aggregated state. Although a conformational ensemble of fibrillar states cannot be ruled out, 2D IR clearly demonstrates that **mxyl-AD** can form parallel β-sheet assemblies, reminiscent of larger amyloid proteins.

Design and Synthesis of Aggregation-Resistant Backbone-Aminated Derivatives of mxyl-AD. The data above support the hypothesis that the **mxyl-AD** macrocycle can engage in native-like hydrophobic cross-β interactions and self-assembly along the fibril axis. We next sought to employ **mxyl-AD** as a template for the design of soluble β-bracelet tau seeding inhibitors that can cap tau fibril growth and block propagation. This required us to incorporate a chemical modification onto **mxyl-AD** that would preclude its ability to self-assemble without disrupting its capacity to adopt the conformation required to bind tau. We therefore designed two backbone N-amino peptide (NAP) derivatives of our tau mimic, **mxyl-NAP1** and **mxyl-NAP2** (Scheme 2). Each of these analogues features a backbone amide substitution that precludes canonical β-sheet H-bonding along one edge of the macrocycle while leaving the other edge intact to engage the tau protein. We previously demonstrated that backbone N-amination within strand regions of hairpin peptide model systems can enhance β-sheet-like conformation and convert aggregation-prone sequences into soluble, aggregation-resistant peptidomimetics.[56,57,36] Both **mxyl-NAP1** and **mxyl-NAP2**, which feature a single backbone N-amino group within the

https://doi.org/10.1021/jacs.3c06830
J. Am. Chem. Soc. 2023, 145, 23131−23142

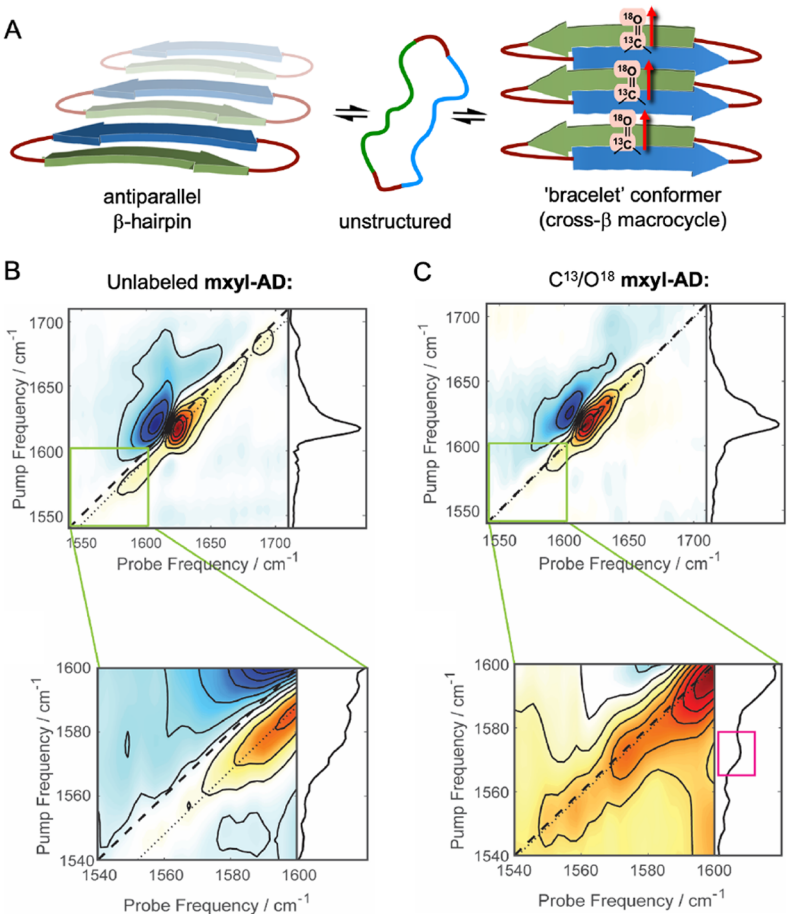

Figure 6. (A) Depiction of the transition from random coil to β-hairpin or β-arch assemblies for macrocyclic bracelets (a linear chain of aligned oscillators for an isotope-labeled carbonyl group is shown for the parallel bracelet conformer). 2D IR spectra of (B) 250 μM unlabeled **mxyl-AD** and (C) V17 $^{13}C/^{18}O$-labeled macrocycle ($^{13}C/^{18}O$-**mxyl-AD**) in deuterated aq PBS buffer. Scaling (8.5×) is provided to increase the visibility of the contour plots. The dashed line marks the diagonal of the spectrum ($\omega_{pump} = \omega_{probe}$), and the panels to the right of each spectrum show a diagonal cut of the spectrum taken along the dotted line. Zoomed inset (in C) reveals the 1573 cm^{-1} peak that appears in the labeled spectrum (boxed in pink).

Scheme 2. Synthesis of mxyl-NAP1 and mxyl-NAP2

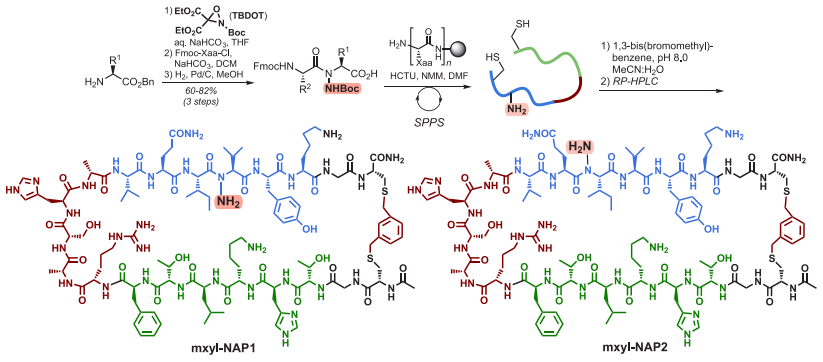

amyloidogenic PHF6 module, were prepared on a solid support starting from Fmoc-protected N-amino dipeptides. As anticipated, both compounds exhibited enhanced solubility in DMSO and aq PBS relative to **mxyl-AD** and did not form mature fibrils, as judged by the ThT assay (Figure S6).

Inhibition of Full-Length Tau Aggregation by mxyl-NAPs in a ThT Assay. To test whether **mxyl-NAPs** effectively inhibit the growth of tau fibrils, we expressed and purified the P301L mutant of 0N4R tau (tau_{P301L}) for evaluation in ThT assays. Tau_{P301L} (5 μM) aggregated upon incubation with heparin over the course of 2 days, leading to a high ThT fluorescence. This fluorescence was significantly attenuated in the presence of 10 μM **mxyl-NAP1** or **mxyl-NAP2** (Figure 7A and B). We also synthesized linear and scrambled controls corresponding to each of the NAP inhibitors (Figure S7). In the case of **mxyl-NAP1**, neither of the controls (**linear-NAP1** or **scrm-NAP1**) showed a significant effect on tau_{P301L} aggregation at 10 μM. Incubation with **scrm-NAP2** led to a

https://doi.org/10.1021/jacs.3c06830
J. Am. Chem. Soc. 2023, 145, 23131−23142

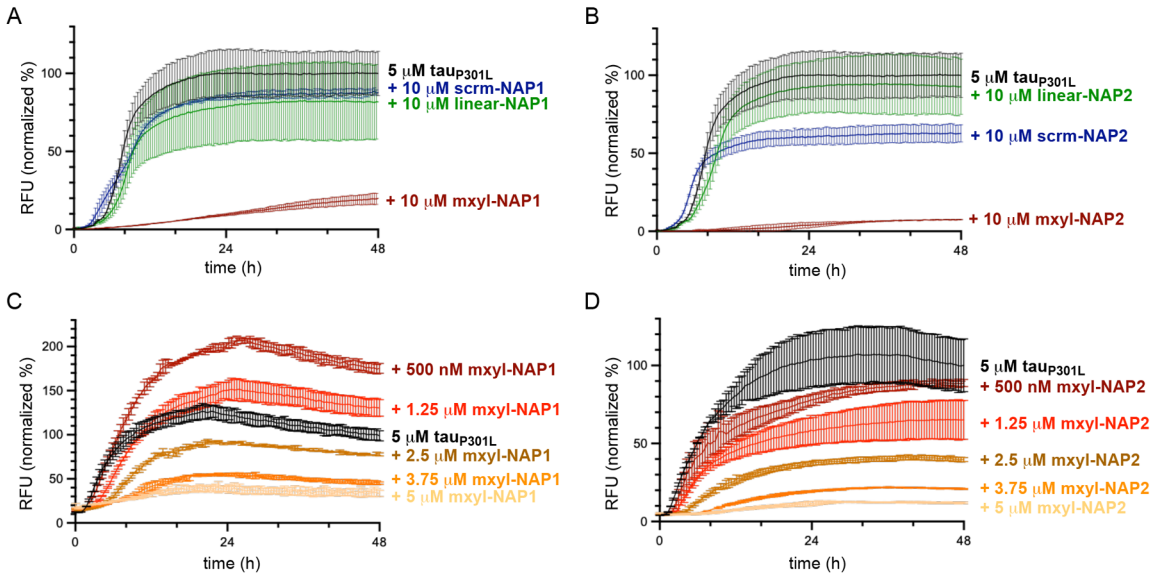

Figure 7. Tau_{P301L} (5 μM) aggregation in the presence of heparin (5 μM), ThT (10 μM), and synthesized compounds. (A) Relative ThT fluorescence of heparin-induced tau_{P301L} alone or in the presence of 10 μM **myxl-NAP1**, **linear NAP-1**, or **scrm-NAP1**. (B) Relative ThT fluorescence of heparin-induced tau_{P301L} alone or in the presence of 10 μM **myxl-NAP2**, **linear NAP-2**, or **scrm-NAP2**. (C, D) Dose-dependent effects of **mxyl-NAP1** and **mxyl-NAP2** on tau_{P301L} aggregation at sub-stoichiometric inhibitor concentrations. Fluorescence intensities for each experiment are normalized to the maximum fluorescence in wells containing only tau_{P301L} and heparin.

modest reduction of tau aggregation by ThT but was still far less effective than that with **mxyl-NAP2**.

We then examined whether **mxyl-NAP1** and **mxyl-NAP2** could effectively inhibit tau_{P301L} aggregation at sub-stoichiometric concentrations. Both compounds exhibited a clear concentration-dependent effect on heparin-induced tau_{P301L} aggregation, including significant inhibition at 0.5× concentration relative to protein (Figure 7C and D). **Mxyl-NAP2** appeared to be the more effective inhibitor, showing clear reduction of aggregation even at 0.25× tau_{P301L} concentration and approximately 90% inhibition at 1× tau_{P301L} concentration. Interestingly, the lowest concentrations of **mxyl-NAP1** tested resulted in a slight enhancement of ThT fluorescence, indicating a possible templating effect. However, **mxyl-NAP1** concentrations of 2.5 μM and above were still effective at suppressing the aggregation of tau_{P301L}.

A pelleting assay was used to confirm the association of **mxyl-NAP2** with tau fibrils. An aliquot of heparin-induced tau_{P301L} fibrils was incubated with **mxyl-NAP2** and pelleted using ultracentrifugation. Depletion of **mxyl-NAP2** in the supernatant relative to control vials lacking tau_{P301L} indicated interaction of the inhibitor with structured tau fibrils or protofibrils (Figure S8). We observed no binding isotherm upon titration of **mxyl-NAP2** into a solution of monomeric tau_{P301L} (Figure S9). Despite its capacity to self-assemble into ThT-positive fibrils, we also tested whether the **mxyl-AD** bracelet, lacking the backbone N-amino group, was capable of inhibiting tau_{P301L} aggregation. Here, we observed a significant enhancement (~350%) of ThT fluorescence in **mxyl-AD**-treated wells (Figure S10), indicating that N-amination is required to convert the macrocyclic AD tau epitope mimic into an inhibitor of aggregation.

Inhibition of Full-Length Tau Fibrilization by mxyl-NAPs in TEM. To confirm the results from ThT assays, we used TEM to visualize tau_{P301L} fibrils in the absence or presence of synthesized NAPs. As expected, heparin-induced tau_{P301L} formed dense networks of mature fibrils (Figure S11). Incubation of 5 μM tau_{P301L} in the presence of heparin and 10 μM **mxyl-NAP1** afforded no elongated fibrils and only sparse areas containing small protofibrillar structures (Figure 8). No fibrils were found in the presence of **mxyl-NAP2**. In contrast, **linear-NAP1**, **scrm-NAP1**, **linear-NAP2**, and **scrm-NAP2** had little effect on the fibrilization of tau_{P301L}, as judged by TEM. Each of the samples treated with these control compounds

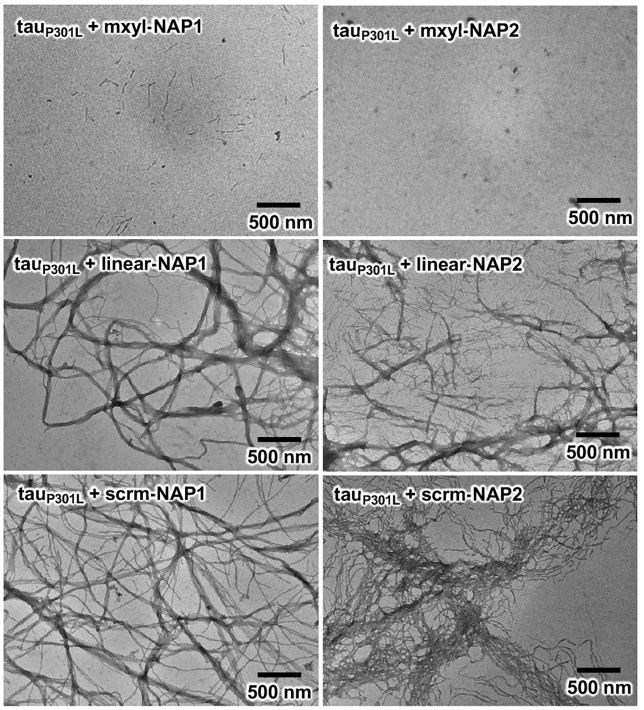

Figure 8. TEM images of heparin-induced tau_{P301L} (5 μM) in the presence of 10 μM **mxyl-NAP1**, **mxyl-NAP2**, and corresponding controls (scale bar = 500 nm).

https://doi.org/10.1021/jacs.3c06830
J. Am. Chem. Soc. 2023, 145, 23131−23142

showed mature fibrils similar to those in the untreated wells. Results from TEM are thus in agreement with ThT fluorescence assays and demonstrate that the inhibitory effect of **mxyl-NAPs** is both macrocycle- and sequence-dependent.

Mxyl-NAPs Inhibit the Seeding Capacity of Full-Length Tau in a Biosensor Cell Assay. The ability to halt the prion-like spread of tau fibrils from diseased to healthy cells using designed molecules remains a considerable challenge. While several compounds demonstrate inhibitory activity against the aggregation of tau (or short peptides derived from tau) *in vitro*, smaller oligomeric forms of tau may still be able to nucleate the growth of endogenous fibrils once taken up by cells. To test whether **mxyl-NAPs** could block this seeding activity, we treated HEK293 biosensor cells that express a tau yellow fluorescent protein fusion (tau-RD[LM]-YFP)[11,58] with tau_{P301L} incubated in the presence or absence of inhibitors. Heparin-induced fibrils of tau_{P301L} grown in the absence of **mxyl-NAPs** led to strong intracellular fluorescence, resulting from endogenous tau-RD(LM)-YFP aggregation. Quantitative brightness threshold-based analysis of puncta within the biosensor cells provided a positive baseline for seed-competent recombinant tau fibrils. For these experiments, we found that tau_{P301L} fibrils grown for 4 days with low-molecular-weight heparin yielded the most active seeds (~60,000 puncta/15,000 cells upon treatment with 190 nM tau_{P301L}; Figure S12). Remarkably, 95 nM **mxyl-NAP1** almost totally blocked the seeding activity of tau_{P301L} when added in the fibril growth stage (Figures 9 and 10). Moreover, **linear-NAP1** and

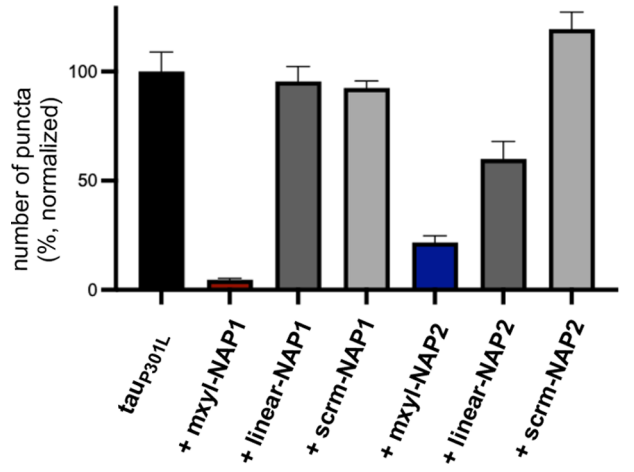

Figure 9. Inhibition of tau_{P301L} (190 nM) seeding activity in HEK293 biosensor cells by 95 nM (A) **mxyl-NAP1**, (B) **mxyl-NAP2**, and the corresponding control NAPs. Puncta counts are normalized to the maximum number from cells treated with only tau_{P301L} fibrils.

scrm-NAP1 at the same concentration had no effect on the seeding capacity of heparin-induced tau_{P301L}, as measured by fluorescent punctate counting. **Mxyl-NAP2** similarly exhibited potent inhibition of tau_{P301L} seeding activity at 95 nM, with control analogues displaying modest or no activity in the biosensor cell assay.

We then established the dose-dependent anti-seeding activity of both **mxyl-NAP1** and **mxyl-NAP2**. Tau_{P301L} (190 nM) treated with either 2 equiv (380 nM) or 0.5 equiv (95 nM) of each inhibitor exhibited significantly reduced ability to seed endogenous tau-RD(LM)-YFP, while lower concentrations were less effective (Figure 11). Data from biosensor cellular assays demonstrate that **mxyl-NAPs** not only impair

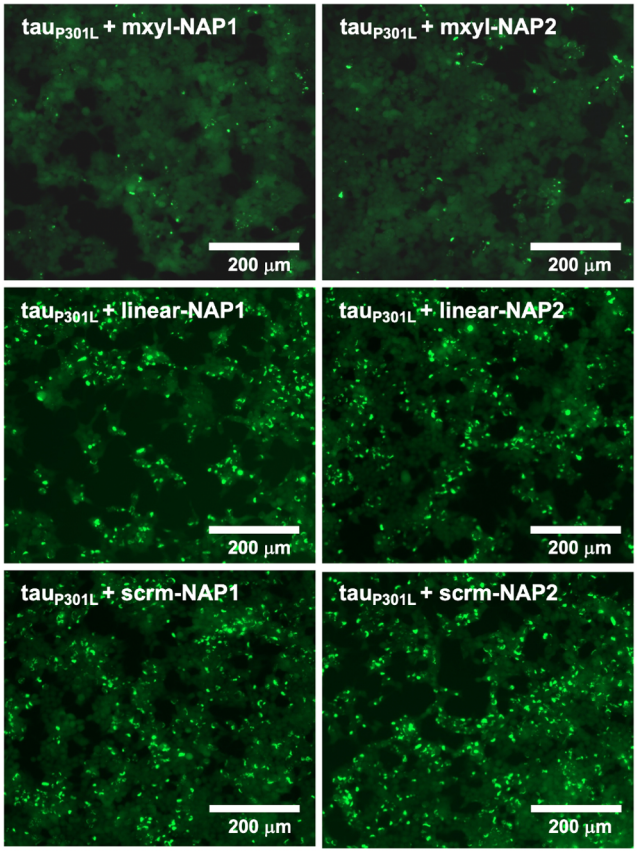

Figure 10. Endogenous tau-RD(LM)-YFP aggregation seeded by 190 nM tau_{P301L} in the presence or absence of 95 nM **mxyl-NAPs**. Representative fluorescence microscopy images of HEK293 biosensor cells at 20× magnification under the FITC channel (scale bars = 200 μm).

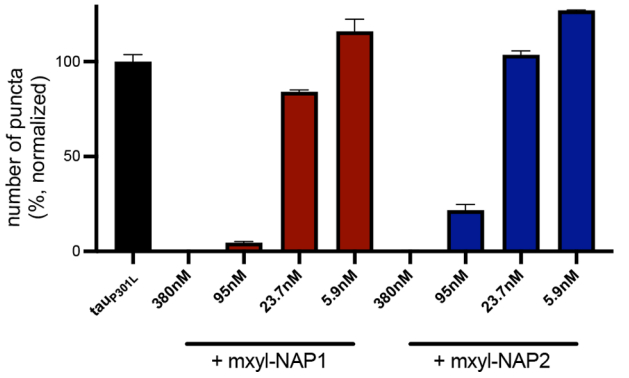

Figure 11. Dose-dependent anti-seeding activity of **mxyl-NAP1** and **mxyl-NAP2** against 190 nM tau_{P301L}. Puncta counts are normalized to the maximum number from cells treated with only tau_{P301L} fibrils.

mature tau fibril growth but also abrogate the formation of smaller seed-competent tau oligomers that may be critical for templated tau propagation across cells.

Mxyl-NAPs Inhibit the Seeding Capacity of AD Tau Derived from Patient Samples. Given that our macrocyclic NAPs were designed based on the amyloidogenic cross-β structure within the tau AD fold, we examined whether these compounds could inhibit the seeding activity of AD tau fibrils. This assay would also assess whether **mxyl-NAPs** are able to cap mature tau fibrils that have already adopted the

https://doi.org/10.1021/jacs.3c06830
J. Am. Chem. Soc. 2023, 145, 23131−23142

conformation observed in high-resolution structures of AD patient samples. Recapitulating the pathological folds encountered in brain tissue using a recombinant protein remains a major challenge. Recent reports described the characterization of an AD tau fold in fibrils grown *in vitro* from a truncated $tau_{297-391}$ construct (dGAE).[59,60] We expressed and purified dGAE and confirmed its aggregation at various concentrations by ThT (Figure S13). However, attempts to seed endogenous tau-RD(LM)-YFP within the biosensor cells with pre-formed dGAE fibrils under various conditions were unsuccessful.

We then turned to post-mortem brain extracts of sarkosyl-insoluble tau from AD patients (Figure 12A). We screened

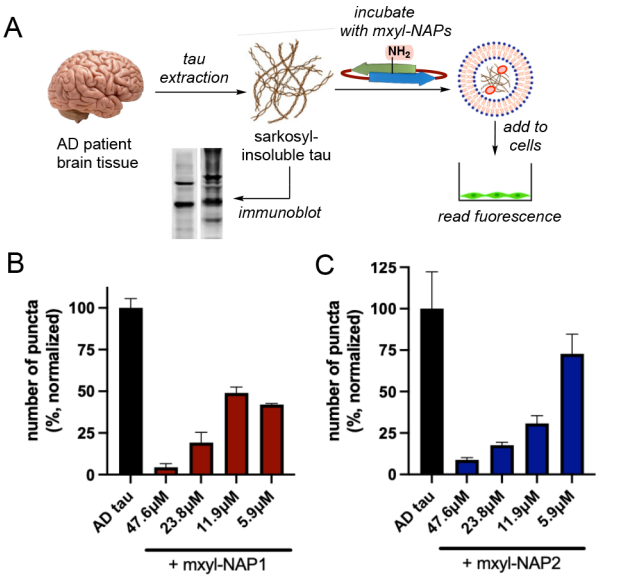

Figure 12. (A) Extraction and cell-based seeding assays with AD tau. Dose-dependent anti-seeding activity of (B) **mxyl-NAP1** and (C) **mxyl-NAP2** against patient-derived extracts of AD tau. Puncta counts are normalized to the maximum number from cells treated with only AD tau fibrils.

four different patient samples for consistent seeding activity in the biosensor cells and selected the strongest patient seed extract to perform experiments with varying concentrations of **mxyl-NAPs** (Figure S14). While the untreated AD-associated tau fibrils induced ~13,000 puncta/15,000 cells, we observed strong inhibition of seeding activity upon incubation with 23.8 and 47.6 μM of **mxyl-NAP1** (Figures 12B and S15). Treatment of 2 μL of patient-derived AD tau extract with lower concentrations of **mxyl-NAP1** (11.9 or 5.9 μM) resulted in less effective inhibition of intracellular tau-RD(LM)-YFP aggregates. **Mxyl-NAP2** exhibited similar dose-dependent reduction of AD tau seeding activity, with >50% inhibitory efficacy at 11.3 μM (Figure 12C). Although we did not observe any qualitative changes in cell morphology upon treatment with **mxyl-NAPs**, we also sought to ensure that the compounds were not inhibiting seeding due to cytotoxicity. MTT assay using HEK293 (biosensor) treated with **mxyl-NAPs** demonstrated >90% cell viability up to 50 μM (Figure S16). These macrocycles exhibited only minimal toxicity toward SH-SY5Y (neuroblastoma) cells at 50 μM and no apparent toxicity at 10 μM.

DISCUSSION

Amyloid folds often feature side-chain interdigitation of β-strand modules that are interspersed throughout each protomer. While the self-assembly of β-sheet-rich amyloids is driven by backbone H-bonding, desolvation and hydrophobic collapse can generate tightly packed core motifs that stabilize amyloid folds in a manner analogous to globular proteins.[61,62,3] Outward-facing side chains may also engage in favorable, in-register π stacking or amide ladder interactions with adjacent protomers along the fibril axis.[63−66] In the current study, we leveraged the naturally occurring cross-β interactions found in the AD fold of tau to design cross-β epitope mimics with amyloidogenic properties. The resulting β-bracelets are distinct from single-strand mimics of the aggregation-prone PHF6 module in that they display additional strand edges and faces to facilitate self-assembly and tau fold recognition.

In the case of AD tau, the PHF6 hexapeptide (residues 306−311) is located distant in primary sequence from its complementary β-strand module (residues 373−378).[38] We therefore sought to address two initial questions in our design: (1) Can the intervening tau residues be replaced with a synthetic β-arch-promoting motif to afford a minimal amyloidogenic peptide, and (2) do the resulting cross-β mimics engage in parallel β-sheet self-assembly similar to full-length tau? Preliminary experiments indicated that a linear cross-β mimic connected through a β-arc pentapeptide did not readily form aggregates or mature fibrils, as monitored by ThT fluorescence or TEM. However, fibril formation was enhanced upon incorporation of select macrocyclic tethers at the peptide termini. We hypothesize that Cys bis-alkylation facilitates adoption of the desired cross-β fold. The fact that a similar enhancement of aggregation was observed with β-bracelets derived from heparin-induced and CBD tau fibril folds suggests that the *m*-xylyl linker supports β-arc conformation within these macrocyclic peptides. Interestingly, even subtle modifications to the linker geometry or composition had a significant impact on the aggregation propensity. This highlights the utility of a divergent bis-alkylation approach and suggests that screening a larger set of electrophiles may yield more optimally constrained cross-β folds.

Our attempts to generate diffraction-quality crystals from *m*-xylyl-linked β-bracelets proved unsuccessful. We obtained a well-resolved ^{1}H NMR spectrum of unaggregated **mxyl-AD** in 9:1 H_2O:D_2O and confirmed its random coil structure by CD spectroscopy (Figure S17). However, the insolubility of fibrillar **mxyl-AD** at concentrations suitable for NMR precluded attempts to determine the solution structure of the self-assembled state. A transition from a random coil to a canonical β-sheet conformation was clearly evident from CD spectroscopy carried out on fibillar **mxyl-AD**. Reported CD spectra from fibrillar tau constructs as well as short peptides derived from the PHF6 and PHF6* motifs can exhibit significant contributions from other secondary structures.[67−70] In contrast, **mxyl-AD** fibrils exhibit a dominant parallel sheet conformation without the need for co-factor-mediated induction. 2D IR spectroscopy with an isotopically labeled derivative of **mxyl-AD** further supports its in-register parallel β-sheet structure following fibrilization.

The PHF6 and PHF6* hexapeptides are required for tau fibrilization and have long served as templates for the structure-based design of tau aggregation inhibitors. Amyloidogenic β-bracelets thus offer an opportunity to develop a new

https://doi.org/10.1021/jacs.3c06830
J. Am. Chem. Soc. 2023, 145, 23131−23142

class of molecules to target tau propagation and seeding. Incorporation of a single backbone N-amino group at the Val or Ile residue in the PHF6 strand rendered the parent macrocycle soluble and resistant to aggregation. The CD spectra of **mxyl-NAP1** and **mxyl-NAP2** indicated a random coil conformation similar to that of pre-fibrillar **mxyl-AD** (Figure S18). This indicates that N-amination is sufficient to block self-assembly but does not enforce the cross-β structure on its own. It is therefore likely that the conformational transition of **mxyl-AD** to a cross-β structure is more dependent on H-bonding between monomers than cross-β side-chain packing. Notably, our efforts to synthesize the analogous N-methylated derivatives were met with poor coupling efficiencies at the tertiary amide site and low crude purities. Isolation of the desired N-methylated products was also attended by the rapid formation of insoluble aggregates, thus precluding their use in subsequent assays.

As with **mxyl-AD**, the tau mimetic properties of our N-aminated derivatives were dependent on both their sequence and their cyclic nature. For example, a striking absence of mature tau fibrils was observed by TEM in the presence of NAP bracelets, while dense networks of fibrils were evident in the presence of sequence-scrambled and acyclic control NAPs. A similar trend was observed in cellular propagation assays, where recombinant tau was rendered incapable of seeding endogenous tau in the presence of **mxyl-NAP1** or **mxyl-NAP2**. N-Aminated β-bracelets were effective inhibitors of recombinant tau aggregation as well as cellular seeding activity, even at sub-stoichiometric concentrations.

Elucidating the role of cell-to-cell tau fibril transmission in pathogenesis will require chemical probes that can inhibit the seeding activity of disease-associated folds. Toward this end, tau seeds extracted from human brain tissue represent the gold standard for evaluating such compounds in cell-based models. We challenged AD patient-derived tau seeds with our NAP bracelets and confirmed dose-dependent inhibition of intracellular tau aggregation. The concentrations needed to block patient-derived tau seeding were considerably higher than those required for monomeric recombinant tau. However, in contrast to purified recombinant tau, the accurate quantitation of seed-competent fibrillar tau from patient samples presents a challenge. Thus, the inhibitor:AD tau ratio required to block propagation cannot be readily determined. Mature fibrils of AD tau, particularly when sonicated prior to cell treatment, produce an array of seed-competent fragments that can serve as nucleation sites for endogenous fibril growth.[34,35] Tau extracted from brain tissue is also part of a complex milieu that includes other forms of post-translationally modified and truncated tau, additional sarkosyl-insoluble proteins, and various biological co-factors. Nevertheless, low micromolar concentrations of our NAP bracelets were sufficient to impair the seeding capacity of AD tau. Additional studies are required to determine if NAP bracelets can inhibit fibril transmission induced by tau derived from patients with other tauopathies or at different stages of disease.

Efforts to recapitulate pathological tau folds *in vitro* are becoming increasingly important, given the structural diversity of tau proteoforms. The scarcity of tau from patient samples and the wide variability in seeding activity of human tau isolates further underscore the need for functional mimics of disease-relevant conformational strains.[71,72] Encouraged by the amyloidogenic properties of our β-bracelets, we examined the seeding capacity of **mxyl-AD** fibrils in the biosensor cells but did not observe the induction of endogenous tau aggregation. Notably, fibrils of the dGAE construct of tau (residues 297−391), which are purported to adopt an AD core fold *in vitro*, also failed to seed endogenous tau in this cellular assay. A possible explanation may lie in the construct of the recipient tau-YFP fusion used in the HEK293 biosensor cells, which feature C-terminal truncation (at residue 372) and lack the cross-β module that is complementary to PHF6 in the AD fold.[11] Reporter cells expressing longer tau isoforms will be useful for investigating the seeding potential of synthetic AD tau mimics.[73,74] The modularity of our β-bracelet approach may also enable the development of seed-competent macrocycles based on other pathological tau strains.

CONCLUSION

Here, we describe the design, synthesis, and biological evaluation of cross-β epitope mimics based on a pathological fold of the tau protein. We utilized β-strand sequences that define a hydrophobic interface within AD tau protomers and appended β-arc linkages to generate a new class of mini-amyloids that self-assemble into parallel β-sheet fibrils. We further demonstrate that the resulting β-bracelets can serve as templates for the design of soluble inhibitors of tau seeding. Our approach lays the groundwork for the development of ligands that recognize and block the propagation of disease-associated conformational tau strains. Beyond targeting tauopathic epitopes, we anticipate that a β-bracelet strategy could be used to develop mimics of other amyloidogenic proteins characterized by intramolecular cross-β interactions. Such compounds could have broad utility as strain-selective ligands, synthetic nucleators, or minimalist models of physiologically relevant amyloid folds.

ASSOCIATED CONTENT

Supporting Information

The Supporting Information is available free of charge at https://pubs.acs.org/doi/10.1021/jacs.3c06830.

Supplementary figures, experimental procedures, synthetic peptide characterization data, and HRMS spectra (PDF)

AUTHOR INFORMATION

Corresponding Author

Juan R. Del Valle − *Department of Chemistry & Biochemistry, University of Notre Dame, Notre Dame, Indiana 46556, United States;* orcid.org/0000-0002-7964-8402; Email: jdelvalle@nd.edu

Authors

Benjamin H. Rajewski − *Department of Chemistry & Biochemistry, University of Notre Dame, Notre Dame, Indiana 46556, United States*

Kamlesh M. Makwana − *Department of Chemistry & Biochemistry, University of Notre Dame, Notre Dame, Indiana 46556, United States*

Isaac J. Angera − *Department of Chemistry & Biochemistry, University of Notre Dame, Notre Dame, Indiana 46556, United States*

Danielle K. Geremia − *Department of Chemistry & Biochemistry, University of Notre Dame, Notre Dame, Indiana 46556, United States*

Anna R. Zepeda − *Department of Chemistry & Biochemistry, University of Notre Dame, Notre Dame, Indiana 46556, United States*

Grace I. Hallinan − *Department of Pathology & Laboratory Medicine and Stark Neurosciences Research Institute, Indiana University School of Medicine, Indianapolis, Indiana 46202, United States*

Ruben Vidal − *Department of Pathology & Laboratory Medicine and Stark Neurosciences Research Institute, Indiana University School of Medicine, Indianapolis, Indiana 46202, United States*

Bernardino Ghetti − *Department of Pathology & Laboratory Medicine and Stark Neurosciences Research Institute, Indiana University School of Medicine, Indianapolis, Indiana 46202, United States*

Arnaldo L. Serrano − *Department of Chemistry & Biochemistry, University of Notre Dame, Notre Dame, Indiana 46556, United States;* orcid.org/0000-0002-7268-1306

Complete contact information is available at: https://pubs.acs.org/10.1021/jacs.3c06830

Notes

The authors declare no competing financial interest.

■ ACKNOWLEDGMENTS

This work was supported by grants from the National Institutes of Health (R01AG074570, U01NS110437, and K99AG078500) and the National Science Foundation (CHE2109008 and CHE2239472). We thank the NCAA for support via the President's Pat Summitt Award honorarium. Fellowship support of B.H.R. was provided by the Indiana Clinical and Translational Institute (TL1 predoctoral fellowship) and the Leahy-Filipi Family Endowment (Warren Center for Drug Discovery at Notre Dame). We thank the Biophysics Instrumentation, Nuclear Magnetic Resonance, Mass Spectrometry, and Warren Center Biological Screening Core Facilities for access to instrumentation, as well as Prof. Yichun Wang (Notre Dame) for use of a CD spectrometer. We are grateful to Prof. Marc Diamond (UT Southwestern) for generously providing tau-RD(LM)-YFP biosensor cells.

■ REFERENCES

(1) Knowles, T. P.; Vendruscolo, M.; Dobson, C. M. The amyloid state and its association with protein misfolding diseases. *Nat. Rev. Mol. Cell Biol.* **2014**, *15*, 384−396.

(2) Iadanza, M. G.; Jackson, M. P.; Hewitt, E. W.; Ranson, N. A.; Radford, S. E. A new era for understanding amyloid structures and disease. *Nat. Rev. Mol. Cell Biol.* **2018**, *19*, 755−773.

(3) Taylor, A. I. P.; Staniforth, R. A. General Principles Underpinning Amyloid Structure. *Front Neurosci* **2022**, *16*, 878869.

(4) von Bergen, M.; Barghorn, S.; Biernat, J.; Mandelkow, E. M.; Mandelkow, E. Tau aggregation is driven by a transition from random coil to beta sheet structure. *Biochim. Biophys. Acta* **2005**, *1739*, 158−166.

(5) Spillantini, M. G.; Goedert, M. Tau pathology and neurodegeneration. *Lancet Neurol* **2013**, *12*, 609−622.

(6) Arendt, T.; Stieler, J. T.; Holzer, M. Tau and tauopathies. *Brain Res. Bull.* **2016**, *126*, 238−292.

(7) Limorenko, G.; Lashuel, H. A. Revisiting the grammar of Tau aggregation and pathology formation: how new insights from brain pathology are shaping how we study and target Tauopathies. *Chem. Soc. Rev.* **2022**, *51*, 513−565.

(8) Kyalu Ngoie Zola, N.; Balty, C.; Pyr dit Ruys, S.; Vanparys, A. A. T.; Huyghe, N. D. G.; Herinckx, G.; Johanns, M.; Boyer, E.; Kienlen-Campard, P.; Rider, M. H.; Vertommen, D.; Hanseeuw, B. J. Specific post-translational modifications of soluble tau protein distinguishes Alzheimer's disease and primary tauopathies. *Nat. Commun.* **2023**, *14*, 3706.

(9) Frost, B.; Jacks, R. L.; Diamond, M. I. Propagation of tau misfolding from the outside to the inside of a cell. *J. Biol. Chem.* **2009**, *284*, 12845−12852.

(10) Kfoury, N.; Holmes, B. B.; Jiang, H.; Holtzman, D. M.; Diamond, M. I. Trans-cellular propagation of Tau aggregation by fibrillar species. *J. Biol. Chem.* **2012**, *287*, 19440−19451.

(11) Sanders, D. W.; Kaufman, S. K.; DeVos, S. L.; Sharma, A. M.; Mirbaha, H.; Li, A.; Barker, S. J.; Foley, A. C.; Thorpe, J. R.; Serpell, L. C.; Miller, T. M.; Grinberg, L. T.; Seeley, W. W.; Diamond, M. I. Distinct tau prion strains propagate in cells and mice and define different tauopathies. *Neuron* **2014**, *82*, 1271−1288.

(12) Gibbons, G. S.; Lee, V. M. Y.; Trojanowski, J. Q. Mechanisms of Cell-to-Cell Transmission of Pathological Tau A Review. *Jama Neurology* **2019**, *76*, 101−108.

(13) Bulic, B.; Pickhardt, M.; Schmidt, B.; Mandelkow, E.-M.; Waldmann, H.; Mandelkow, E. Development of Tau Aggregation Inhibitors for Alzheimer's Disease. *Angew. Chem., Int. Ed.* **2009**, *48*, 1740−1752.

(14) Soeda, Y.; Takashima, A. New Insights Into Drug Discovery Targeting Tau Protein. *Front. Mol. Neurosci.* **2020**, *13*, 590896.

(15) Wang, L.; Bharti; Kumar, R.; Pavlov, P. F.; Winblad, B. Small molecule therapeutics for tauopathy in Alzheimer's disease: Walking on the path of most resistance. *Eur. J. Med. Chem.* **2021**, *209*, 112915.

(16) Aillaud, I.; Funke, S. A. Tau Aggregation Inhibiting Peptides as Potential Therapeutics for Alzheimer Disease. *Cell Mol. Neurobiol* **2023**, *43*, 951−961.

(17) Armiento, V.; Spanopoulou, A.; Kapurniotu, A. Peptide-Based Molecular Strategies To Interfere with Protein Misfolding, Aggregation, and Cell Degeneration. *Angew. Chem., Int. Ed.* **2020**, *59*, 3372−3384.

(18) Dammers, C.; Yolcu, D.; Kukuk, L.; Willbold, D.; Pickhardt, M.; Mandelkow, E.; Horn, A. H.; Sticht, H.; Malhis, M. N.; Will, N.; Schuster, J.; Funke, S. A. Selection and Characterization of Tau Binding D-Enantiomeric Peptides with Potential for Therapy of Alzheimer Disease. *PLoS One* **2016**, *11*, No. e0167432.

(19) Belostozky, A.; Richman, M.; Lisniansky, E.; Tovchygrechko, A.; Chill, J. H.; Rahimipour, S. Inhibition of tau-derived hexapeptide aggregation and toxicity by a self-assembled cyclic d,l-α-peptide conformational inhibitor. *Chem. Commun. (Camb)* **2018**, *54*, 5980−5983.

(20) Zhang, X.; Zhang, X.; Zhong, M.; Zhao, P.; Guo, C.; Li, Y.; Wang, T.; Gao, H. Selection of a d-Enantiomeric Peptide Specifically Binding to PHF6 for Inhibiting Tau Aggregation in Transgenic Mice. *ACS Chem. Neurosci.* **2020**, *11*, 4240−4253.

(21) Malhis, M.; Kaniyappan, S.; Aillaud, I.; Chandupatla, R. R.; Ramirez, L. M.; Zweckstetter, M.; Horn, A. H. C.; Mandelkow, E.; Sticht, H.; Funke, S. A. Potent Tau Aggregation Inhibitor D-Peptides Selected against Tau-Repeat 2 Using Mirror Image Phage Display. *Chembiochem* **2021**, *22*, 3049−3059.

(22) Gorantla, N. V.; Sunny, L. P.; Rajasekhar, K.; Nagaraju, P. G.; Cg, P. P.; Govindaraju, T.; Chinnathambi, S. Amyloid-β-Derived Peptidomimetics Inhibits Tau Aggregation. *ACS Omega* **2021**, *6*, 11131−11138.

(23) Zhu, L.; Xu, L.; Wu, X.; Deng, F.; Ma, R.; Liu, Y.; Huang, F.; Shi, L. Tau-Targeted Multifunctional Nanoinhibitor for Alzheimer's Disease. *ACS Appl. Mater. Interfaces* **2021**, *13*, 23328−23338.

(24) Kondo, K.; Ikura, T.; Tanaka, H.; Fujita, K.; Takayama, S.; Yoshioka, Y.; Tagawa, K.; Homma, H.; Liu, S.; Kawasaki, R.; Huang, Y.; Ito, N.; Tate, S. I.; Okazawa, H. Hepta-Histidine Inhibits Tau Aggregation. *ACS Chem. Neurosci.* **2021**, *12*, 3015−3027.

(25) Aillaud, I.; Kaniyappan, S.; Chandupatla, R. R.; Ramirez, L. M.; Alkhashrom, S.; Eichler, J.; Horn, A. H. C.; Zweckstetter, M.; Mandelkow, E.; Sticht, H.; Funke, S. A. A novel D-amino acid peptide

with therapeutic potential (ISAD1) inhibits aggregation of neurotoxic disease-relevant mutant Tau and prevents Tau toxicity in vitro. *Alzheimers Res. Ther* **2022**, *14*, 15.
(26) Danis, C.; Dupré, E.; Zejneli, O.; Caillierez, R.; Arrial, A.; Bégard, S.; Mortelecque, J.; Eddarkaoui, S.; Loyens, A.; Cantrelle, F. X.; Hanoulle, X.; Rain, J. C.; Colin, M.; Buée, L.; Landrieu, I. Inhibition of Tau seeding by targeting Tau nucleation core within neurons with a single domain antibody fragment. *Mol. Ther* **2022**, *30*, 1484−1499.
(27) Altendorf, T.; Gering, I.; Santiago-Schübel, B.; Aghabashlou Saisan, S.; Tamgüney, G.; Tusche, M.; Honold, D.; Schemmert, S.; Hoyer, W.; Mohrlüder, J.; Willbold, D. Stabilization of Monomeric Tau Protein by All D-Enantiomeric Peptide Ligands as Therapeutic Strategy for Alzheimer's Disease and Other Tauopathies. *Int. J. Mol. Sci.* **2023**, *24*, 2161−2188.
(28) von Bergen, M.; Friedhoff, P.; Biernat, J.; Heberle, J.; Mandelkow, E. M.; Mandelkow, E. Assembly of tau protein into Alzheimer paired helical filaments depends on a local sequence motif ((306)VQIVYK(311)) forming beta structure. *Proc. Natl. Acad. Sci. U. S. A.* **2000**, *97*, 5129−5134.
(29) Barghorn, S.; Davies, P.; Mandelkow, E. Tau paired helical filaments from Alzheimer's disease brain and assembled in vitro are based on beta-structure in the core domain. *Biochemistry* **2004**, *43*, 1694−1703.
(30) Pandey, G.; Morla, S.; Kumar, S.; Ramakrishnan, V. Modulation of tau protein aggregation using 'Trojan' sequences. *Biochim Biophys Acta Gen Subj* **2020**, *1864*, 129569.
(31) Zheng, J.; Liu, C.; Sawaya, M. R.; Vadla, B.; Khan, S.; Woods, R. J.; Eisenberg, D.; Goux, W. J.; Nowick, J. S. Macrocyclic β-sheet peptides that inhibit the aggregation of a tau-protein-derived hexapeptide. *J. Am. Chem. Soc.* **2011**, *133*, 3144−3157.
(32) Zheng, J.; Baghkhanian, A. M.; Nowick, J. S. A Hydrophobic Surface Is Essential To Inhibit the Aggregation of a Tau-Protein-Derived Hexapeptide. *J. Am. Chem. Soc.* **2013**, *135*, 6846−6852.
(33) Wang, C. K.; Northfield, S. E.; Huang, Y. H.; Ramos, M. C.; Craik, D. J. Inhibition of tau aggregation using a naturally-occurring cyclic peptide scaffold. *Eur. J. Med. Chem.* **2016**, *109*, 342−349.
(34) Seidler, P. M.; Boyer, D. R.; Rodriguez, J. A.; Sawaya, M. R.; Cascio, D.; Murray, K.; Gonen, T.; Eisenberg, D. S. Structure-based inhibitors of tau aggregation. *Nat. Chem.* **2018**, *10*, 170−176.
(35) Seidler, P. M.; Boyer, D. R.; Murray, K. A.; Yang, T. P.; Bentzel, M.; Sawaya, M. R.; Rosenberg, G.; Cascio, D.; Williams, C. K.; Newell, K. L.; Ghetti, B.; DeTure, M. A.; Dickson, D. W.; Vinters, H. V.; Eisenberg, D. S. Structure-based inhibitors halt prion-like seeding by Alzheimer's disease-and tauopathy-derived brain tissue samples. *J. Biol. Chem.* **2019**, *294*, 16451−16464.
(36) Makwana, K. M.; Sarnowski, M. P.; Miao, J.; Lin, Y.-S.; Del Valle, J. R. N-Amination Converts Amyloidogenic Tau Peptides into Soluble Antagonists of Cellular Seeding. *ACS Chem. Neurosci.* **2021**, *12*, 3928−3938.
(37) Lövestam, S.; Scheres, S. H. W. High-throughput cryo-EM structure determination of amyloids. *Faraday Discuss.* **2022**, *240*, 243−260.
(38) Fitzpatrick, A. W. P.; Falcon, B.; He, S.; Murzin, A. G.; Murshudov, G.; Garringer, H. J.; Crowther, R. A.; Ghetti, B.; Goedert, M.; Scheres, S. H. W. Cryo-EM structures of tau filaments from Alzheimer's disease. *Nature* **2017**, *547*, 185−190.
(39) Scheres, S. H.; Zhang, W.; Falcon, B.; Goedert, M. Cryo-EM structures of tau filaments. *Curr. Opin Struct Biol.* **2020**, *64*, 17−25.
(40) Shi, Y.; Zhang, W.; Yang, Y.; Murzin, A. G.; Falcon, B.; Kotecha, A.; van Beers, M.; Tarutani, A.; Kametani, F.; Garringer, H. J.; Vidal, R.; Hallinan, G. I.; Lashley, T.; Saito, Y.; Murayama, S.; Yoshida, M.; Tanaka, H.; Kakita, A.; Ikeuchi, T.; Robinson, A. C.; Mann, D. M. A.; Kovacs, G. G.; Revesz, T.; Ghetti, B.; Hasegawa, M.; Goedert, M.; Scheres, S. H. W. Structure-based classification of tauopathies. *Nature* **2021**, *598*, 359−363.
(41) Goedert, M. Cryo-EM structures of τ filaments from human brain. *Essays Biochem* **2021**, *65*, 949−959.
(42) Hoogerhout, P.; Kamphuis, W.; Brugghe, H. F.; Sluijs, J. A.; Timmermans, H. A.; Westdijk, J.; Zomer, G.; Boog, C. J.; Hol, E. M.; van den Dobbelsteen, G. P. A cyclic undecamer peptide mimics a turn in folded Alzheimer amyloid β and elicits antibodies against oligomeric and fibrillar amyloid and plaques. *PLoS One* **2011**, *6*, No. e19110.
(43) Spanopoulou, A.; Heidrich, L.; Chen, H. R.; Frost, C.; Hrle, D.; Malideli, E.; Hille, K.; Grammatikopoulos, A.; Bernhagen, J.; Zacharias, M.; Rammes, G.; Kapurniotu, A. Designed Macrocyclic Peptides as Nanomolar Amyloid Inhibitors Based on Minimal Recognition Elements. *Angew. Chem., Int. Ed. Engl.* **2018**, *57*, 14503−14508.
(44) Zhang, W.; Falcon, B.; Murzin, A. G.; Fan, J.; Crowther, R. A.; Goedert, M.; Scheres, S. H. W. Heparin-induced tau filaments are polymorphic and differ from those in Alzheimer's and Pick's diseases. *eLife* **2019**, *8*, No. e43584.
(45) Zhang, W.; Tarutani, A.; Newell, K. L.; Murzin, A. G.; Matsubara, T.; Falcon, B.; Vidal, R.; Garringer, H. J.; Shi, Y.; Ikeuchi, T.; Murayama, S.; Ghetti, B.; Hasegawa, M.; Goedert, M.; Scheres, S. H. W. Novel tau filament fold in corticobasal degeneration. *Nature* **2020**, *580*, 283−287.
(46) Hennetin, J.; Jullian, B.; Steven, A. C.; Kajava, A. V. Standard conformations of beta-arches in beta-solenoid proteins. *J. Mol. Biol.* **2006**, *358*, 1094−1105.
(47) Kajava, A. V.; Baxa, U.; Steven, A. C. Beta arcades: recurring motifs in naturally occurring and disease-related amyloid fibrils. *FASEB J.* **2010**, *24*, 1311−1319.
(48) Thomas, N. C.; Bartlett, G. J.; Woolfson, D. N.; Gellman, S. H. Toward a Soluble Model System for the Amyloid State. *J. Am. Chem. Soc.* **2017**, *139*, 16434−16437.
(49) Micsonai, A.; Wien, F.; Kernya, L.; Lee, Y.-H.; Goto, Y.; Réfrégiers, M.; Kardos, J. Accurate secondary structure prediction and fold recognition for circular dichroism spectroscopy. *Proc. Natl. Acad. Sci. U. S. A.* **2015**, *112*, E3095−E3103.
(50) Guo, Y.; Wang, S.; Du, H.; Chen, X.; Fei, H. Silver Ion-Histidine Interplay Switches Peptide Hydrogel from Antiparallel to Parallel β-Assembly and Enables Controlled Antibacterial Activity. *Biomacromolecules* **2019**, *20*, 558−565.
(51) Richaud, A. D.; Roche, S. P. Structure−Property Relationship Study of N-(Hydroxy)Peptides for the Design of Self-Assembled Parallel β-Sheets. *Journal of Organic Chemistry* **2020**, *85*, 12329−12342.
(52) Hamm, P.; Zanni, M. *Concepts and Methods of 2D Infrared Spectroscopy*; Cambridge University Press: Cambridge, 2011.
(53) Woys, A. M.; Almeida, A. M.; Wang, L.; Chiu, C.-C.; McGovern, M.; de Pablo, J. J.; Skinner, J. L.; Gellman, S. H.; Zanni, M. T. Parallel β-Sheet Vibrational Couplings Revealed by 2D IR Spectroscopy of an Isotopically Labeled Macrocycle: Quantitative Benchmark for the Interpretation of Amyloid and Protein Infrared Spectra. *J. Am. Chem. Soc.* **2012**, *134*, 19118−19128.
(54) Lomont, J. P.; Ostrander, J. S.; Ho, J.-J.; Petti, M. K.; Zanni, M. T. Not All β-Sheets Are the Same: Amyloid Infrared Spectra, Transition Dipole Strengths, and Couplings Investigated by 2D IR Spectroscopy. *J. Phys. Chem. B* **2017**, *121*, 8935−8945.
(55) Buchanan, L. E.; Dunkelberger, E. B.; Tran, H. Q.; Cheng, P.-N.; Chiu, C.-C.; Cao, P.; Raleigh, D. P.; de Pablo, J. J.; Nowick, J. S.; Zanni, M. T. Mechanism of IAPP amyloid fibril formation involves an intermediate with a transient β-sheet. *Proc. Natl. Acad. Sci. U. S. A.* **2013**, *110*, 19285−19290.
(56) Sarnowski, M. P.; Kang, C. W.; Elbatrawi, Y. M.; Wojtas, L.; Del Valle, J. R. Peptide N-Amination Supports β-Sheet Conformations. *Angew. Chem., Int. Ed.* **2017**, *56*, 2083−2086.
(57) Sarnowski, M. P.; Pedretty, K. P.; Giddings, N.; Woodcock, H. L.; Del Valle, J. R. Synthesis and beta-sheet propensity of constrained N-amino peptides. *Bioorg. Med. Chem.* **2018**, *26*, 1162−1166.
(58) Holmes, B. B.; Furman, J. L.; Mahan, T. E.; Yamasaki, T. R.; Mirbaha, H.; Eades, W. C.; Belaygorod, L.; Cairns, N. J.; Holtzman, D. M.; Diamond, M. I. Proteopathic tau seeding predicts tauopathy in vivo. *Proc. Natl. Acad. Sci. U. S. A.* **2014**, *111*, E4376.

(59) Al-Hilaly, Y. K.; Foster, B. E.; Biasetti, L.; Lutter, L.; Pollack, S. J.; Rickard, J. E.; Storey, J. M. D.; Harrington, C. R.; Xue, W.-F.; Wischik, C. M.; Serpell, L. C. Tau (297−391) forms filaments that structurally mimic the core of paired helical filaments in Alzheimer's disease brain. *FEBS Lett.* **2020**, *594*, 944−950.
(60) Lövestam, S.; Koh, F. A.; van Knippenberg, B.; Kotecha, A.; Murzin, A. G.; Goedert, M.; Scheres, S. H. W. Assembly of recombinant tau into filaments identical to those of Alzheimer's disease and chronic traumatic encephalopathy. *Elife* **2022**, *11*, No. e76494.
(61) Dill, K. A. Dominant forces in protein folding. *Biochemistry* **1990**, *29*, 7133−7155.
(62) Fitzpatrick, A. W.; Knowles, T. P. J.; Waudby, C. A.; Vendruscolo, M.; Dobson, C. M. Inversion of the Balance between Hydrophobic and Hydrogen Bonding Interactions in Protein Folding and Aggregation. *PLOS Computational Biology* **2011**, *7*, No. e1002169.
(63) Perutz, M. F.; Johnson, T.; Suzuki, M.; Finch, J. T. Glutamine repeats as polar zippers: their possible role in inherited neurodegenerative diseases. *Proc. Natl. Acad. Sci. U. S. A.* **1994**, *91*, 5355−5358.
(64) Gazit, E. A possible role for π-stacking in the self-assembly of amyloid fibrils. *FASEB J.* **2002**, *16*, 77−83.
(65) Makin, O. S.; Atkins, E.; Sikorski, P.; Johansson, J.; Serpell, L. C. Molecular basis for amyloid fibril formation and stability. *Proc. Natl. Acad. Sci. U. S. A.* **2005**, *102*, 315−320.
(66) Nelson, R.; Sawaya, M. R.; Balbirnie, M.; Madsen, A.; Riekel, C.; Grothe, R.; Eisenberg, D. Structure of the cross-beta spine of amyloid-like fibrils. *Nature* **2005**, *435*, 773−778.
(67) Frost, B.; Ollesch, J.; Wille, H.; Diamond, M. I. Conformational Diversity of Wild-type Tau Fibrils Specified by Templated Conformation Change*. *J. Biol. Chem.* **2009**, *284*, 3546−3551.
(68) Andreasen, M.; Skeby, K. K.; Zhang, S.; Nielsen, E. H.; Klausen, L. H.; Frahm, H.; Christiansen, G.; Skrydstrup, T.; Dong, M.; Schiøtt, B.; Otzen, D. The importance of being capped: Terminal capping of an amyloidogenic peptide affects fibrillation propensity and fibril morphology. *Biochemistry* **2014**, *53*, 6968−6980.
(69) Fanni, A. M.; Vander Zanden, C. M.; Majewska, P. V.; Majewski, J.; Chi, E. Y. Membrane-mediated fibrillation and toxicity of the tau hexapeptide PHF6. *J. Biol. Chem.* **2019**, *294*, 15304−15317.
(70) Honisch, C.; Torni, F.; Hussain, R.; Ruzza, P.; Siligardi, G. Effect of Trehalose and Ceftriaxone on the Stability of Aggregating-Prone Tau Peptide Containing PHF6* Sequence: An SRCD Study. *International Journal of Molecular Sciences* **2022**, *23*, 2932.
(71) Dujardin, S.; Commins, C.; Lathuiliere, A.; Beerepoot, P.; Fernandes, A. R.; Kamath, T. V.; De Los Santos, M. B.; Klickstein, N.; Corjuc, D. L.; Corjuc, B. T.; Dooley, P. M.; Viode, A.; Oakley, D. H.; Moore, B. D.; Mullin, K.; Jean-Gilles, D.; Clark, R.; Atchison, K.; Moore, R.; Chibnik, L. B.; Tanzi, R. E.; Frosch, M. P.; Serrano-Pozo, A.; Elwood, F.; Steen, J. A.; Kennedy, M. E.; Hyman, B. T. Tau molecular diversity contributes to clinical heterogeneity in Alzheimer's disease. *Nature medicine* **2020**, *26*, 1256−1263.
(72) Xu, H.; O'Reilly, M.; Gibbons, G. S.; Changolkar, L.; McBride, J. D.; Riddle, D. M.; Zhang, B.; Stieber, A.; Nirschl, J.; Kim, S.-J.; Hoxha, K.-h.; Brunden, K. R.; Schellenberg, G. D.; Trojanowski, J. Q.; Lee, V. M. Y. In vitro amplification of pathogenic tau conserves disease-specific bioactive characteristics. *Acta Neuropathologica* **2021**, *141*, 193−215.
(73) Tarutani, A.; Lövestam, S.; Zhang, X.; Kotecha, A.; Robinson, A. C.; Mann, D. M. A.; Saito, Y.; Murayama, S.; Tomita, T.; Goedert, M.; Scheres, S. H. W.; Hasegawa, M. Cryo-EM structures of tau filaments from SH-SY5Y cells seeded with brain extracts from cases of Alzheimer's disease and corticobasal degeneration. *FEBS Open Bio* **2023**, *13*, 1394.
(74) Lester, E.; Ooi, F. K.; Bakkar, N.; Ayers, J.; Woerman, A. L.; Wheeler, J.; Bowser, R.; Carlson, G. A.; Prusiner, S. B.; Parker, R. Tau aggregates are RNA-protein assemblies that mislocalize multiple nuclear speckle components. *Neuron* **2021**, *109*, 1675−1691.e1679.

https://doi.org/10.1021/jacs.3c06830
J. Am. Chem. Soc. 2023, 145, 23131−23142